Caffeine Supplementation and FOXM1 Inhibition Enhance the Antitumor Effect of Statins in Neuroblastoma

Gia-Buu Tran[1,2,3], Jane Ding[1,2], Bingwei Ye[4], Mengling Liu[5], Yajie Yu[5], Yunhong Zha[5], Zheng Dong[6,7], Kebin Liu[8], Sunil Sudarshan[2,9], and Han-Fei Ding[1,2]

ABSTRACT

High-risk neuroblastoma exhibits transcriptional activation of the mevalonate pathway that produces cholesterol and nonsterol isoprenoids. A better understanding of how this metabolic reprogramming contributes to neuroblastoma development could help identify potential prevention and treatment strategies. Here, we report that both the cholesterol and nonsterol geranylgeranyl-pyrophosphate branches of the mevalonate pathway are critical to sustain neuroblastoma cell growth. Blocking the mevalonate pathway by simvastatin, a cholesterol-lowering drug, impeded neuroblastoma growth in neuroblastoma cell line xenograft, patient-derived xenograft (PDX), and TH-MYCN transgenic mouse models. Transcriptional profiling revealed that the mevalonate pathway was required to maintain the FOXM1-mediated transcriptional program that drives mitosis. High FOXM1 expression contributed to statin resistance and led to a therapeutic vulnerability to the combination of simvastatin and FOXM1 inhibition. Furthermore, caffeine synergized with simvastatin to inhibit the growth of neuroblastoma cells and PDX tumors by blocking statin-induced feedback activation of the mevalonate pathway. This function of caffeine depended on its activity as an adenosine receptor antagonist, and the A2A adenosine receptor antagonist istradefylline, an add-on drug for Parkinson's disease, could recapitulate the synergistic effect of caffeine with simvastatin. This study reveals that the FOXM1-mediated mitotic program is a molecular statin target in cancer and identifies classes of agents for maximizing the therapeutic efficacy of statins, with implications for treatment of high-risk neuroblastoma.

Significance: Caffeine treatment and FOXM1 inhibition can both enhance the antitumor effect of statins by blocking the molecular and metabolic processes that confer statin resistance, indicating potential combination therapeutic strategies for neuroblastoma.

See related commentary by Stouth et al., p. 2091

Introduction

The mevalonate pathway uses acetyl coenzyme A (acetyl-CoA) to generate sterols, such as cholesterol, and nonsterol isoprenoids (**Fig. 1A**; refs. 1, 2). Cholesterol is a precursor for producing steroid hormones, oxysterols, bile acids, and vitamin D. In addition, it is a structural component of cellular membranes, accounting for approximately 25 mole percent of plasma membrane lipids (3). Thus, its continuous production is required for cell proliferation. Nonsterol isoprenoids include farnesyl-pyrophosphate (FPP) and geranylgeranyl-pyrophosphate (GGPP), both of which are used for prenylation and activation of the RAS superfamily of GTPases. Moreover, isoprenoids are precursors for producing dolichol, heme A, ubiquinone, and coenzyme Q, which have important functions in many cellular processes. Increased production of mevalonate derivatives is a common feature of cancer metabolism and targeting the mevalonate pathway is increasingly recognized as a cancer therapeutic strategy (4, 5).

Sterol regulatory element-binding protein 2 (SREBP2), encoded by *SREBF2*, has a major role in transcriptional activation of the mevalonate pathway. It is synthesized as an inactive precursor that forms a complex with SREBP-cleavage activating protein (SCAP). When the sterol level is high, the SCAP-SREBP2 complex binds tightly to the endoplasmic reticulum (ER) resident insulin-induced gene (INSIG) 1 or 2 protein, leading to SREBP2 retention in the ER. When sterol is insufficient, the SCAP-SREBP2 complex dissociates from INSIGs and translocates to the Golgi, where SREBP2 is cleaved, releasing its N-terminal transcription factor domain, which then enters the nucleus and activates the transcription of mevalonate pathway genes. This end-product feedback control is crucial for maintaining sterol homeostasis and for holding the mevalonate pathway in check (6).

Neuroblastoma is a pediatric cancer of the sympathetic nervous system. Approximately half of all neuroblastoma cases are high-risk, which have a poor overall survival rate, despite remarkable advances in neuroblastoma therapy in recent years (7, 8). A major focus of our research is to identify metabolic vulnerabilities of high-risk neuroblastoma for therapeutic exploitation (9). We have shown previously that transcriptional activation of the mevalonate pathway is a key feature of metabolic reprogramming in high-risk neuroblastoma, which sustains the proliferation and survival of neuroblastoma cells (10). Studies from other laboratories have also reported that

[1]Division of Molecular and Cellular Pathology, Department of Pathology, University of Alabama at Birmingham, Birmingham, Alabama. [2]O'Neal Comprehensive Cancer Center, Birmingham, Alabama. [3]Faculty of Pharmacy, Ton Duc Thang University, Ho Chi Minh City, Vietnam. [4]Georgia Prevention Institute, Augusta University, Augusta, Georgia. [5]Institute of Neural Regeneration and Repair and Department of Neurology, The First Hospital of Yichang, Three Gorges University College of Medicine, Yichang, China. [6]Department of Cell Biology and Anatomy, Augusta University, Augusta, Georgia. [7]Charlie Norwood VA Medical Center, Augusta, Georgia. [8]Department of Biochemistry and Molecular Biology, Medical College of Georgia, Augusta University, Augusta, Georgia. [9]Department of Urology, Heersink School of Medicine, University of Alabama at Birmingham, Birmingham, Alabama.

G.B. Tran and J. Ding contributed equally to this article.

Corresponding Author: Han-Fei Ding, Division of Molecular and Cellular Pathology, Department of Pathology, University of Alabama at Birmingham, WTI 602D, 1824 6th Avenue South, Birmingham, AL 35294-3300. Phone 205-934-7670; E-mail: hding@uabmc.edu

Cancer Res 2023;83:2248–61

doi: 10.1158/0008-5472.CAN-22-3450

This open access article is distributed under the Creative Commons Attribution-NonCommercial-NoDerivatives 4.0 International (CC BY-NC-ND 4.0) license.

©2023 The Authors; Published by the American Association for Cancer Research

blocking the mevalonate pathway inhibits neuroblastoma cell growth, triggers apoptosis, and disrupts cellular metabolism (11–14). These observations suggest that the mevalonate pathway is crucial for the development of high-risk neuroblastoma.

In the current study, we assessed the therapeutic potential of targeting the mevalonate pathway by statins, a class of cholesterol-lowering drugs that inhibit the rate-limiting enzyme 3-hydroxy-3-methylglutaryl-CoA reductase (HMGCR; **Fig. 1A**). Further, we conducted profiling of statin-responsive genes for rational development of drug combinations to enhance the antitumor efficacy of statins.

Materials and Methods

Cell lines

All neuroblastoma cell lines used in this study and their culture conditions have been described in detail previously (15). The patient-derived xenograft (PDX) cell lines COG-N-496 (RRID:CVCL_LF61) and COG-N-519 (RRID:CVCL_LF62) were obtained from Childhood Cancer Repository (Texas Tech University Health Sciences Center) and cultured in IMDM (Gibco, 12440–053) supplemented with 20% FBS (Thermo Fisher Scientific, FB12999102) and 1x insulin-transferrin-selenium (Gibco, 41400–045). CHO-K1 cells (ATCC CCL-61, RRID:CVCL_0214) were cultured in DME/F-12 1:1 (HyClone SH30023) supplemented with 10% FBS, 1x nonessential amino acids (Gibco, 11140–050), and 1x GlutaMAX (Gibco, 35050–061). Cell lines from commercial sources and cell line repositories were authenticated using short tandem repeat profiling and upon receiving, large frozen stocks were made to ensure against contaminations by other cell lines. Neuroblastoma cell lines were monitored regularly by immunoblotting and immunofluorescence for high-level nuclear expression of MYCN and/or the specific neuroblastoma marker PHOX2B (16, 17). All cell lines were used within 10 passages after reviving from frozen stocks and were free of *Mycoplasma* contamination as determined by DAPI staining every 3 months. Cell images were captured using an EVOS M5000 Imaging System (Invitrogen).

Drugs and small molecules

Adenosine (Tocris, 3624), FTI-277 (Selleckchem, S7465), GGTI-298 (Tocris, 2430), istradefylline (KW-6002, MedChemExpress HY-10888), NB-598 maleate (AdooQ, A15180–10), simvastatin (Selleckchem, S1792), pitavastatin (Selleckchem, S1759), thapsigargin (Sigma-Aldrich, 586005), thiostrepton (Sigma-Aldrich, 598226), and YM-53601 (Cayman, 18113) were dissolved in DMSO (Thermo Fisher Scientific BP231), and stock solutions were aliquoted and stored at −80°C. FPP (Cayman 63250) and GGPP (Cayman 63330) were supplied as a solution of methanol:NH_4OH (70:30) and stored at −20°C. Baclofen (MedChemExpress, HY-B0007) and caffeine (Tocris, 2793) were dissolved in H_2O and mevalonolactone (Sigma-Aldrich M4667) was diluted with H_2O and stored at −20°C. Cells were treated with individual or combinations of drugs or small molecules at indicated concentrations for various times and collected for trypan blue exclusion assay, qRT-PCR or immunoblotting.

In vivo drug treatment and xenograft assay

The animal experiments were conducted at the Augusta University and University of Alabama at Birmingham and approved by Institutional Animal Care and Use Committees of Medical College of Georgia, Augusta University, and University of Alabama at Birmingham. Six-week-old NOD/SCID male and female mice (NOD.Cg-Prkdc^{scid}/J, 001303, RRID:IMSR_JAX:001303) from The Jackson Laboratory were used in all human neuroblastoma cell line xenograft and PDX studies. Tumor volume was measured every other day using a digital caliper and estimated using the equation $V = (L \times W^2)/2$. Animals were euthanized when their tumors reach ∼1.0 cm in any diameter.

TH-MYCN mice - simvastatin study

Thirty-one-day-old male and female *TH-MYCN* transgenic mice (129×1/SvJ-Tg(TH-MYCN)41Waw/Nci, NCI Mouse Repository 01XD2, RRID:MGI:5009550) were randomly assigned to 2 groups and treated with vehicle (200 μL 50% PEG 300 in PBS) or simvastatin at 40 mg/kg body weight by gavage every other day for 90 days (45 doses). Mice were monitored for tumor progression until euthanasia was required according to criteria described in the animal protocols.

NOD/SCID xenografts - shFDFT1 study

BE(2)-C cells expressing either shGFP or shFDFT1–25 were suspended in 100 μL Hanks' Balanced Salt Solution (HBSS; Gibco 14170–112) and injected subcutaneously into both sides of the flank (2 sites per mouse) at 3×10^6 cells per injection site.

NOD/SCID xenografts - simvastatin and thiostrepton combination study

BE(2)-C cells in 100 μL HBSS were injected subcutaneously into both sides of the flank at 4×10^6 cells per injection site. Following injection, mice were randomly assigned to control and treatment groups ($n = 5$ per group) and treated 6 days per week with: (i) vehicle (200 μL 50% PEG 300 in PBS by gavage), (ii) simvastatin at 50 mg/kg body weight (simvastatin in 100 μL 50% PEG 300 in PBS by gavage), (iii) thiostrepton at 50 mg/kg body weight (thiostrepton in 100 μL 50% PEG 300 in PBS by gavage), or (iv) simvastatin and thiostrepton at 50 mg/kg body weight (drugs in 200 μL 50% PEG 300 in PBS by gavage). Treatment began on the day of inoculation and continued for 50 days. The thiostrepton dose was chosen on the basis of the previous report that intraperitoneal injection of thiostrepton at 40 or 80 mg/kg had no significant effect on mouse body weight (18).

NOD/SCID PDX - simvastatin and caffeine combination study

Neuroblastoma PDX COG-N-519x was obtained from Childhood Cancer Repository. It was derived originally from a stage 4 neuroblastoma tumor with *MYCN* amplification following chemotherapy (19). Upon receiving, the strained PDX cells were collected by centrifugation, resuspended in 100 μL HBSS, and injected subcutaneously into the flank of a NOD/SCID mouse. The resultant secondary xenograft was collected, minced, treated with ACK buffer (150 mmol/L NH4Cl, 10 mmol/L KHCO3, 0.1 mmol/L EDTA, pH 7.3) to lyse red blood cells, passed through a 70-μm cell strainer, and collected by centrifugation. The cells were then resuspended in HBSS and injected subcutaneously into NOD/SCID mice to generate tertiary xenografts. Strained cells from tertiary xenografts were suspended in cell-freezing media (10% DMSO to 90% FBS) and stored in liquid nitrogen until use. For *in vivo* drug combination treatment, COG-N-519x cells in 100 μL HBSS were injected subcutaneously into both sides of the flank at 4×10^6 cells per injection site. Following injection, mice were randomly assigned to control and treatment groups ($n = 6$ per group) and treated daily with: (i) vehicle (drinking with autoclaved water and feeding with 200 μL 50% PEG 300 in PBS by gavage), (ii) caffeine at ∼80 mg/kg body weight per day (drinking with caffeinated water 0.4 g/L and feeding with 200 μL 50% PEG 300 in PBS by gavage), (iii) simvastatin at 50 mg/kg body weight (drinking with autoclaved water and feeding with simvastatin in 200 μL 50% PEG 300 in PBS by gavage), (iv) caffeine at ∼40 mg/kg body weight per day (drinking with

caffeinated water 0.2 g/L) plus simvastatin at 50 mg/kg body weight, or (v) caffeine at ∼80 mg/kg body weight per day (caffeinated water 0.4 g/L) plus simvastatin at 50 mg/kg body weight. Treatment began on the day of tumor inoculation and continued for 38 days until all mice in the vehicle control group were euthanized. The study was terminated on day 67 postinoculation.

IHC

Tumor tissues were fixed in 10% neutral buffered formalin, embedded in paraffin blocks, and sectioned at 5 μm. Slides with tissue section were baked overnight at 60°C and then deparaffinized in 3 changes of xylene and hydrated using graded concentrations of ethanol to deionized water. The tissue sections were treated for 5 minutes in 0.01 mol/L sodium citrate buffer (pH 6) in a pressure cooker for antigen retrieval, washed in deionized water, and then transferred into 0.05 mol/L Tris-based solution in 0.15 mol/L NaCl with 0.1% v/v Triton-X-100, pH 7.6 (TBST). Endogenous peroxidase was blocked with 3% hydrogen peroxide for 15 minutes. Slides were incubated with 5% normal goat serum (Sigma, G9023) for 60 minutes at room temperature to minimize further nonspecific background staining and then incubated at 4°C overnight with a rabbit anti-cleaved caspase-3 (1:500, Cell Signaling Technology, 9661, RRID:AB_2341188). After washing with TBST, sections were then incubated with the goat anti-rabbit IgG H&L secondary antibody conjugated with HRP (Abcam, ab6721, 1:1,000, RRID:AB_955447). ImmPACT DAB Peroxidase (HRP) Substrate Kit (Vector Laboratories SK4105) was used as the chromogen and hematoxylin (Richard-Allen Scientific 7221) as the counterstain.

Patient data

Patient data used in this study were described previously (20, 21). All survival and gene expression correlation analyses were conducted online using R2: Genomics Analysis and Visualization Platform (https://hgserver1.amc.nl/cgi-bin/r2/main.cgi), and the resulting figures and *P* values were downloaded.

Overexpression and RNA interference

Human *FOXM1* coding sequence in pOTB7-FOXM1 (Open Biosystems) was subcloned into the retroviral vector pRetroX-Tight-pur (Clontech 632106) for inducible FOXM1 expression in the absence of tetracycline or doxycycline (tetoff-FOXM1). Retroviruses were produced in 293FT cells using the packaging plasmids pHDM-G and pMD.MLVogp (22). Cell lines with tetoff-FOXM1 were maintained in media containing 0.5 μg/mL doxycycline. For FOXM1 induction, cells were cultured in the absence of doxycycline for various times. Lentiviral constructs for overexpressing human FDFT1 (pLX304-FDFT1, HsCD00438174) and SQLE (pLX304-SQLE, HsCD00441716) were obtained from DNASU, and lentiviral pLKO.1-based shRNA constructs shFDFT1–25 (TRCN0000036325), shFDFT1–28 (TRCN0000036328), shFOXM1–43 (TRCN0000015543), shFOXM1–44 (TRCN0000015544), shFOXM1–84 (TRCN0000273984), shSQLE-53 (TRCN0000046153), and shSQLE-57 (TRCN0000046157) were obtained from Sigma-Aldrich. Lentiviruses were produced in 293FT cells using the packaging plasmids pLP1 (RRID:Addgene_22614), pLP2, and pLP/VSVG (Thermo Fisher Scientific K497500). Retroviral and lentiviral infection of cells were conducted according to standard procedures.

qRT-PCR

TRIzol (Thermo Fisher Scientific, 15596026) was used for isolation of total RNA from cells, iScript Advanced cDNA Synthesis Kit (Bio-Rad, 172–5038) for reverse transcription, and 2X SYBR green qPCR master mix (Bimake, B21203) for qRT-PCR using an iQ5 real-time PCR system (Bio-Rad) with primers against various genes (Supplementary Table S1). Data were normalized to β2 microglobulin (B2M) mRNA levels. All primer pairs were verified by melting curve analysis following qRT-PCR, with each primer pair showing a single desired amplification peak.

Immunoblotting

Cell lysates were prepared using standard SDS sample buffer, and nuclear extracts prepared using a NE-PER nuclear extraction kit (Pierce Chemical 78833). Protein concentrations were determined using a Bio-Rad Protein Assay Kit II (5000002). Proteins (20–50 μg) were separated on SDS-polyacrylamide gels, transferred to nitrocellulose membranes, and probed with the following primary antibodies: rabbit anti-ACSS2 (1:1,000, Cell Signaling Technology, 3658, RRID:AB_2222710), mouse anti-CCNB1 (1:200, Santa Cruz, sc-245, RRID:AB_627338), rabbit anti-cleaved caspase-3 (1:1,000, Cell Signaling Technology, 9664, RRID:AB_2070042), rabbit anti-FDFT1 (1:1,000, Proteintech, 13128–1-AP, RRID:AB_2294094), mouse anti-FOXM1 (1:200, Santa Cruz, sc-166709, RRID:AB_2106326), rabbit anti-GAPDH (1:1,000, Santa Cruz, sc-25778, RRID:AB_10167668), mouse anti-HMGCS1 (1:500, Santa Cruz, sc-166763, RRID:AB_2118317), rabbit anti-LC3B (1:1,000, Cell Signaling Technology, 3868, RRID:AB_2137707), mouse anti-MYCN (B8.4.B, 1:400, Santa Cruz, sc-53993, RRID:AB_831602), mouse anti-SQLE (1:500, Santa Cruz, sc-271651, RRID:AB_10708249), mouse anti-SREBP2 (IgG-7D4, 1:10, ATCC, CRL-2198), rabbit anti-β-actin (1:2,000, Invitrogen, MA5–15739), and mouse anti–α-tubulin (B-5–1-2, 1:5,000, Sigma-Aldrich, T5168, RRID:AB_477579). Horseradish peroxidase-conjugated goat anti-mouse (Jackson ImmunoResearch, 115–035–146, RRID:AB_2307392) and goat anti-rabbit IgG (Jackson ImmunoResearch, 111–035–046, RRID:AB_2337939) were used as secondary antibodies. Immunoblots were visualized using a Clarity Western ECL Substrate Kit (Bio-Rad 1705061) and quantified with Amersham ImageQuant 80 (Cytiva) or ImageJ (version 1.53k).

Microarray

Total RNA was isolated using TRIzol from three biological replicates of SMS-KCNR cells treated for 30 hours with DMSO (vehicle), 5 μmol/L simvastatin, or 5 μmol/L simvastatin plus 2 mmol/L mevalonate. Microarray was performed using the Human Gene 2.0 ST microarray chip (Affymetrix Human Gene Connectome, RRID:SCR_002628). The Partek Genomics Suite (RRID:SCR_011860) was used to normalize data, determine the significance by ANOVA, and calculate fold changes. Gene ontology (GO) analysis by DAVID (RRID:SCR_001881) and gene set enrichment analysis (GSEA; RRID:SCR_003199) were performed as described (23). The Gene Expression Omnibus (GEO; RRID:SCR_005012) accession number for the microarray data reported in this paper is GSE215949.

Synergy analysis

Cells in 6 well plates at 60% to 70% confluence were treated with simvastatin and/or small-molecule inhibitors or chemical compounds for 48 hours. Cell viability was assessed via trypan blue exclusion assay. Dose–response curves for each compound or combination of compounds were generated, and the IC_{50}s were determined using Prism version 9.4 (GraphPad, RRID:SCR_002798). The percentage viability at different concentrations was used as readout, and the synergistic effect of each pair compound combination on cell viability was analyzed using SynergyFinder 3.0 (https://synergyfinder.fimm.fi,

RRID:SCR_019318; ref. 24), and the outlier data were determined by cNMF algorithm (25). The summary synergy score and synergy maps (two-dimensional plots) of compound combination were generated using HSA or Bliss independence models with correction for estimation of drug combination synergy (26). Synergy scores less than −10 indicate that the interaction between the two drugs is likely to be antagonistic, scores from −10 to 10 indicate an additive effect, and scores higher than 10 indicate a synergistic effect.

Cholesterol assay

Cellular cholesterol levels were measured using the Fluorometric Total Cholesterol Assay kit from Cell Biolabs (STA-390). Briefly, cells were washed 3 times with cold PBS, followed by extraction for 30 minutes with a solution of chloroform:isopropanol:NP-40 (7:11:0.1) at 200 μL per 10^6 cells. The extract was transferred to a microtube, vortexed, and centrifuged for 10 minutes at 15,000 × *g*. The liquid (organic phase) was transferred to a new microtube and dried by vacuum centrifugation. The resulting lipid pellet was dissolved in 1X assay diluent, followed by cholesterol assay according to the manufacturer's instruction using a BioTek Synergy LX multi-mode microplate reader (Agilent).

ER Ca^{2+} assay

The assay was performed essentially as described (27). Cells at 50% to 60% confluence were transfected with pcDNA-D1ER (Addgene, 36325, RRID:Addgene_36325) that expresses a fluorescence resonance energy transfer (FRET)-based ER Ca^{2+} sensor composed of an ER-resident calcium binding protein linked to a fluorescent protein. The sensor shows increased green fluorescence intensity upon Ca^{2+} binding (28). One day after transfection, cells were treated with vehicle (H_2O or DMSO), caffeine at 200 μmol/L or Istradefylline (KW-6002 at 5 μmol/L for 24 hours and imaged with an EVOS M5000 Imaging System. Fluorescence intensity was quantified using ImageJ (RRID: SCR_003070, version 1.53k).

Statistics

Quantitative data are presented as mean ± SD ($n = 4$) unless indicated otherwise and were analyzed for statistical significance by unpaired, two-tailed Student *t* test or ANOVA (one-way or two-way). Dose–response curves of drugs and small-molecule inhibitors were fitted with the "log(inhibitor) vs. response (three parameters)". For animal studies, the log-rank test was used to account for mouse survival by the end of animal experiments. Unless otherwise stated, all statistical analyses were conducted using GraphPad Prism 9.4.0 (RRID:SCR_002798) for Mac. Statistical significance was assigned as *, $P < 0.05$; **, $P < 0.01$; ***, $P < 0.001$; ****, $P < 0.0001$.

Data availability

Microarray data reported in this study have been deposited in the GEO (RRID:SCR_005012) under the accession number GSE215949. The patient data analyzed in this study were obtained from R2 Genomics Analysis and Visualization Platform (https://hgserver1.amc.nl/cgi-bin/r2/main.cgi). All other raw data are available upon request from the corresponding author.

Results

Targeting the mevalonate pathway is a therapeutic strategy against high-risk neuroblastoma

To investigate the therapeutic potential of targeting the mevalonate pathway in neuroblastoma, we determined the IC_{50} of simvastatin and pitavastatin against a panel of neuroblastoma cell lines (Supplementary Fig. S1A and S1B). The resultant IC_{50} values were in the range of 0.1 to ∼5 micromoles (Supplementary Fig. S1C). Next, we tested the antitumor effect of simvastatin in *TH-MYCN* transgenic mice (29), a widely used animal model for high-risk neuroblastoma with *MYCN* amplification (30, 31). Neuroblastoma development in *TH-MYCN* mice begins during the first 2 to 3 weeks after birth, which is characterized by the formation of multifocal hyperplasia in sympathetic ganglia (16, 32). Simvastatin treatment of *TH-MYCN* mice was started on postnatal day 31 based on the reasoning that drugs are most effective against tumors of smaller volume (33). *TH-MYCN* mice were given simvastatin at 40 mg/kg every other day by oral gavage for 90 days (45 doses), which significantly reduced tumor incidence and increased the overall survival of *TH-MYCN* mice relative to the vehicle control mice (**Fig. 1B**). Consistent with the previous reports of cell-based studies (12, 13), tumors from *TH-MYCN* mice treated with simvastatin showed markedly increased apoptosis as determined by IHC staining of cleaved caspase-3 (**Fig. 1C** and **D**). Together, these findings demonstrate that the mevalonate pathway is critical for tumor cell survival in the *TH-MYCN* mouse model and is a potential therapeutic target for high-risk neuroblastoma.

The GGPP branch contributes to neuroblastoma cell growth

The mevalonate pathway branches into various biosynthetic routes, producing sterols and nonsterol mevalonate derivatives (**Fig. 1A**). Nonsterol reactions generate FPP and GGPP for prenylation and activation of the RAS, RHO, and RAB families of proteins (**Fig. 1A**; ref. 34). To determine if FPP- or GGPP-mediated prenylation contributes to the survival and proliferation of neuroblastoma cells, we treated neuroblastoma cell lines with FTI-277, an inhibitor of protein farnesyltransferase beta (FNTB), or GGTI-298, an inhibitor of protein geranylgeranyltransferase (PGGT1B), which blocks FPP- and GGPP-mediated prenylation, respectively. Treatment with FTI-277 had no effect (Supplementary Fig. S1D), whereas GGTI-298 treatment significantly inhibited cell survival and proliferation, showing IC_{50} values in the ranges of low micromoles (Supplementary Fig. S1E). To further assess which of these branches mediates the inhibitory effect of simvastatin on neuroblastoma cell growth, we treated the *MYCN*-amplified neuroblastoma cell line BE(2)-C cells with simvastatin in the absence or presence of supplemental mevalonate, FPP or GGPP. Mevalonate completely and GGPP partially abrogated the growth inhibitory effect of simvastatin, whereas FPP failed to show any impact (Supplementary Fig. S1F). Collectively, these data provide evidence that both GGPP and cholesterol branches are critical for the survival and growth of neuroblastoma cells.

The cholesterol branch promotes neuroblastoma cell growth

We next focused our study on the cholesterol branch. The conversion of FPP to squalene is the first committed step in utilizing mevalonate for cholesterol synthesis, which is catalyzed by farnesyl-diphosphate farnesyltransferase 1 (FDFT1; **Fig. 1A**). Analysis of the gene expression profiling data from a cohort of patients with neuroblastoma ($n = 498$, the SEQC dataset; ref. 20) revealed that higher expression of FDFT1 is significantly associated with high-risk neuroblastoma and worse prognosis in patients with neuroblastoma (Supplementary Fig. S2A and S2B), suggesting that increased activation of the cholesterol branch is part of the metabolic reprogramming during high-risk neuroblastoma development. In support of this notion, increasing FDFT1 expression in both *MYCN*-amplified (SMS-KCNR) and non-*MYCN* (SK-N-AS and SHEP1) neuroblastoma cell lines promoted growth (Supplementary Fig. S2C and S2D). In addition,

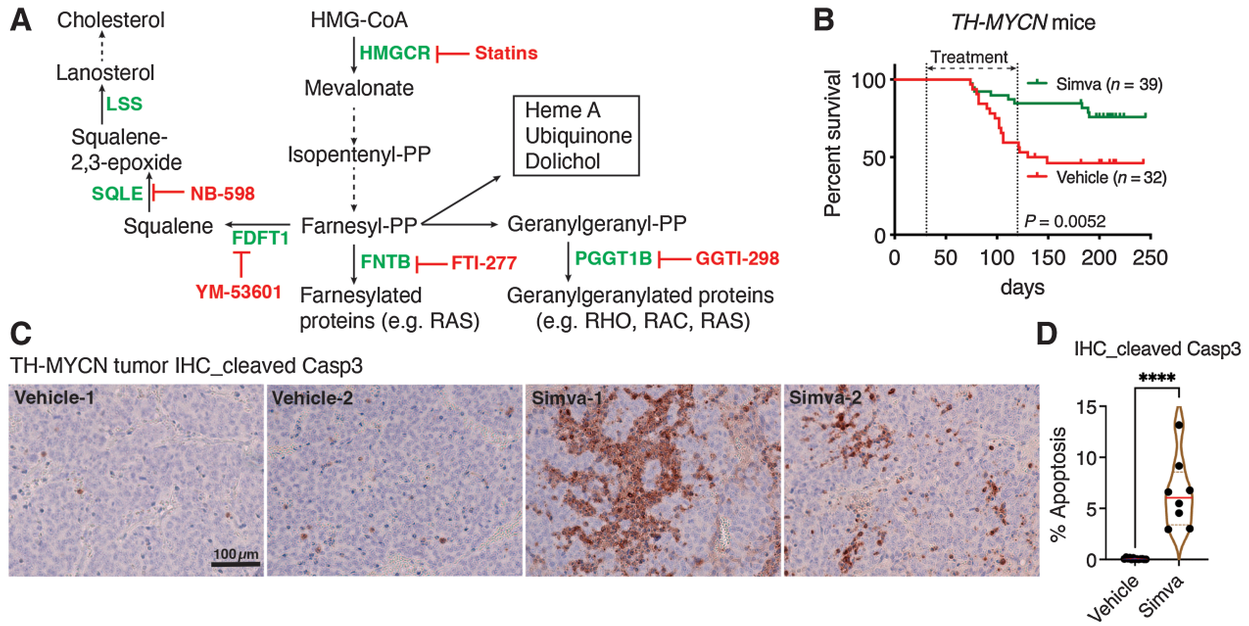

Figure 1.

The mevalonate pathway is a therapeutic target in neuroblastoma. **A,** The mevalonate pathway with indicated key enzymes and their inhibitors. **B,** Kaplan–Meier survival curves for TH-MYCN mice treated with vehicle or simvastatin at 40 mg/kg by gavage every other day for 90 days (45 doses). Log-rank test *P* value is indicated. Treatment was started on postnatal day 31 and ended on day 120. **C,** Representative images of IHC staining of cleaved caspase-3 in tumors from TH-MYCN mice treated with vehicle or simvastatin. **D,** Violin plot of apoptosis levels quantified as areas of cleaved caspase-3–positive staining in 8 to 13 IHC images (200×) from tumors treated with vehicle ($n = 3$) or simvastatin ($n = 2$). *P* values were determined by one-way ANOVA. ****, $P < 0.0001$.

we depleted FDFT1 expression using two lentiviral constructs expressing shRNA sequences targeting different regions of the FDFT1 gene, shFDFT1–25 and shFDFT1–28 (Supplementary Fig. S2E). Knockdown of FDFT1 expression markedly inhibited the proliferation of both *MYCN*-amplified and non-*MYCN* neuroblastoma cell lines (Supplementary Fig. S2F). As a complementary approach, we treated BE(2)-C and SK-N-AS neuroblastoma cell lines with YM-53601, a small-molecule inhibitor of FDFT1. YM-53601 treatment inhibited neuroblastoma cell growth (Supplementary Fig. S2G). Moreover, FDFT1 inhibition or knockdown induced apoptosis, as evidenced by increased levels of cleaved caspase-3, and autophagy, as evidenced by increased LC3B-II production (Supplementary Fig. S2H–S2I), suggesting a key role of cholesterol production in sustaining the survival of neuroblastoma cells.

Consistent with the cell growth data, knockdown of FDFT1 expression markedly impeded the growth of BE(2)-C xenografts in immunodeficient mice and prolonged the survival of xenograft-bearing mice (Supplementary Fig. S2J–S2K).

To further assess the functional significance of the cholesterol branch in neuroblastoma, we investigated the rate-limiting enzyme of the cholesterol branch squalene epoxidase (SQLE) that converts squalene to 2,3-epoxysqualene (**Fig. 1A**). Higher SQLE expression is significantly associated with high-risk neuroblastoma and worse prognosis in patients with neuroblastoma (SEQC and NRC datasets; Supplementary Fig. S3A–S3B; refs. 20, 21). Overexpression of SQLE increased cellular cholesterol levels and enhanced neuroblastoma cell growth (Supplementary Fig. S3C–S3E). We also conducted SQLE knockdown studies with neuroblastoma cells using two independent lentiviral shRNA constructs, shSQLE-53 and shSQLE-57 (Supplementary Fig. S3F). SQLE depletion significantly reduced the proliferation of neuroblastoma cell lines (Supplementary Fig. S3G). We obtained essentially the same results with the SQLE inhibitor NB-598, which inhibited neuroblastoma cell growth with IC_{50} values of 0.5–1 micromoles (Supplementary Fig. S3H).

Taken together, the data presented above demonstrate that increased activation of cholesterol biosynthesis is crucial to sustain the survival and growth of neuroblastoma cell lines *in vitro* and *in vivo*, suggesting that enzymes in the cholesterol branch are potential therapeutic targets for high-risk neuroblastoma.

Simvastatin downregulates mitotic genes

To gain a molecular understanding of the antitumor effect of statins, we performed microarray gene expression profiling of *MYCN*-amplified SMS-KCNR cells treated for 30 hours with vehicle (DMSO), simvastatin (5 μmol/L), or simvastatin (5 μmol/L) plus mevalonate (2 mmol/L). The profiling identified a total of 601 simvastatin-responsive genes (≥±1.50 fold, $P < 0.05$), with 275 genes being upregulated and 326 genes downregulated (Supplementary Table S2). GO analysis revealed that genes downregulated by simvastatin were highly enriched for GO terms associated with mitotic processes and sympathetic nervous system development (Supplementary Fig. S4A; Supplementary Table S3). GSEA generated similar results, showing that the gene sets for mitosis and the FOXM1 pathway were significantly enriched with most of the genes downregulated by simvastatin (Supplementary Fig. S4B and S4C). We confirmed the microarray data by qRT-PCR, showing that simvastatin treatment downregulated the mRNA expression of FOXM1 and its target genes involved in M phase progression (Supplementary Fig. S4D). In addition, we observed that simvastatin treatment reduced the protein levels of FOXM1 and CCNB1

(cyclin B1) in whole cell extracts (WCE), as well as FOXM1 levels in nuclear extracts (Supplementary Fig. S4E and S4F). As reported previously (35, 36), the FOXM1 inhibitor thiostrepton (FOXM1i) decreased nuclear FOXM1 protein levels (Supplementary Fig. S4F). Importantly, supplemental mevalonate fully restored the expression of FOXM1 and mitotic genes, as determined by qRT-PCR, immunoblotting, and microarray gene expression profiling (Supplementary Fig. S4D–S4G; Supplementary Table S4), demonstrating that simvastatin represses the expression of mitotic genes by blocking the mevalonate pathway. These findings reveal an important role of mevalonate metabolism in driving the expression of mitotic genes for cell-cycle progression.

FOXM1 regulates the sensitivity of neuroblastoma cells to simvastatin

FOXM1 target genes drive M phase progression (37) and neuroblastoma development (38, 39). To determine whether downregulation of mitotic genes is a mechanism for simvastatin to inhibit neuroblastoma cell growth, we generated neuroblastoma cell lines with inducible FOXM1 expression in the absence of doxycycline. FOXM1 overexpression increased its target gene expression, for example, CCNB1 (**Fig. 2A**) and conferred resistance to simvastatin (**Fig. 2B**). Conversely, knockdown of FOXM1 expression by shRNA (**Fig. 2C**) sensitized BE(2)-C cells to simvastatin, showing higher levels of growth inhibition than the additive effects of FOXM1 knockdown and simvastatin treatment (**Fig. 2D**). These data suggest that reduced mitotic gene expression is a key mechanism by which simvastatin suppresses neuroblastoma cell growth. Further, these findings suggest that high FOXM1 expression is a potential mechanism for resistance to statins.

The observation that FOXM1 knockdown sensitizes cells to simvastatin provides a rationale for combining statins and drugs that target FOXM1 or mitosis. We tested the idea by combining simvastatin and thiostrepton, a small-molecule inhibitor that represses FOXM1 expression and blocks FOXM1 binding to its target gene promoters and enhancers (35, 36). We used the Bliss independence reference model to analyze the combinatorial effect of simvastatin and thiostrepton, which could be synergistic (Bliss score >10), antagonistic (<−0), or additive (−10 to 10; ref. 24). Our analysis showed an average Bliss score of 8.3 for BE(2)-C cells and 4.6 for IMR5 cells (**Fig. 2E**; Supplementary Fig. S4H), indicating an overall additive effect. However, synergy was observed when the two drugs were used at low concentrations: The highest Bliss score was 23.6 for BE(2)-C and 23.9 for IMR5 cells when simvastatin at 2.5 μmol/L was combined with thiostrepton in the range of 0.5 to 1.0 μmol/L (**Fig. 2E**; Supplementary Fig. S4H). This was confirmed in single-dose combination studies that showed higher levels of growth inhibition than the additive effects of the two drugs, as determined by the Bliss model (Supplementary Fig. S4I).

We further tested the drug combination in NOD/SCID mice carrying BE(2)-C xenografts. The mice were randomly assigned to 4 groups and treated with vehicle, thiostrepton (FOXM1i) at 50 mg/kg body weight by gavage, simvastatin at 50 mg/kg by gavage, or a combination of thiostrepton and simvastatin. Compared with the vehicle control group, thiostrepton or simvastatin alone significantly reduced the tumor growth and extended the survival of tumor-bearing mice, and the combination treatment further reduced tumor incidence and mortality (**Fig. 2F** and **G**). The treatment had no significant effect on the mouse body weight (Supplementary Fig. S4J). In addition, IHC staining of xenograft sections revealed that thiostrepton or simvastatin alone induced significant levels of apoptosis, which were further increased by the drug combination (**Fig. 2H** and **I**).

Together, these observations suggest that statin-mediated downregulation of mitotic genes could be exploited for therapy in combination with drugs that block M phase progression.

Statins induce feedback activation of the mevalonate pathway

In agreement with previous reports (40, 41), GO analysis of genes upregulated by simvastatin revealed significant enrichments of the GO terms for cholesterol and sterol biosynthetic processes (Supplementary Fig. S5A; Supplementary Table S5). GSEA produced similar findings and further showed the upregulation of *SREBF* (coding for SREBP) target genes (Supplementary Fig. S5B). Detailed examination of the mevalonate pathway revealed that most of the pathway genes were upregulated following simvastatin treatment (Supplementary Fig. S5C; Supplementary Table S2). We confirmed the microarray data by qRT-PCR analysis of multiple neuroblastoma cell lines treated with simvastatin or pitavastatin (Supplementary Fig. S5D–S5F). The upregulation was abrogated by supplemental mevalonate (Supplementary Fig. S5D), demonstrating that the statin-induced feedback response was triggered by inhibiting HMGCR. Immunoblot analysis further demonstrated that the feedback response led to increased protein expression of mevalonate pathway enzymes, including HMGCS1 and FDFT1 (Supplementary Fig. S5G–S5H).

SREBP2 has a major role in transcriptional activation of the mevalonate pathway. Statin treatment resulted in a modest, but significant, increase in *SREBP2* mRNA expression in neuroblastoma cell lines (Supplementary Fig. S5C, S5E, and S5F). Using the hamster CHO-K1 cell line as a model (42), we were able to demonstrate that statin treatment promoted the processing of Srebp2, leading to increased production of the N-terminal transcription factor domain of Srebp2 (Supplementary Fig. S5I).

In addition, immunoblot analysis revealed that knockdown of SQLE expression induced HMGCS1 and FDFT1 (Supplementary Fig. S5J), indicating that blocking cholesterol biosynthesis is a major mechanism for triggering the feedback activation of the mevalonate pathway.

Interestingly, statin treatment also induced ACSS2 at both mRNA and protein levels (Supplementary Fig. S5C–S5H). ACSS2 is a cytoplasmic enzyme that converts acetate to acetyl-CoA (Supplementary Fig. S5C), suggesting that the statin-induced feedback response also increases the supply of acetyl-CoA to the mevalonate pathway.

Caffeine abrogates the statin-induced feedback response and synergizes with simvastatin to suppress neuroblastoma cell and PDX growth

It is increasingly recognized that the statin-induced feedback activation of the mevalonate pathway weakens its antitumor effect (40, 41). Identifying agents that block the feedback response may enhance statin-based cancer therapy. It was recently reported that caffeine can block ER stress-induced SREBP2 activation in liver cancer cell lines (27). In agreement with the finding, we found that caffeine could block statin-induced Srebp2 processing and activation in the CHO-K1 cell model (**Fig. 3A**). In neuroblastoma cell lines, caffeine suppressed the statin-induced feedback response, reducing the upregulation of mevalonate pathway enzymes at mRNA and protein levels (**Fig. 3B** and **C**).

The above observations prompted us to investigate whether caffeine could enhance the anti-growth effect of simvastatin by blocking the feedback response. Combination of simvastatin and caffeine at single doses showed higher levels of growth inhibition than the additive effects of the two drugs in the neuroblastoma PDX COG-N-519 cells

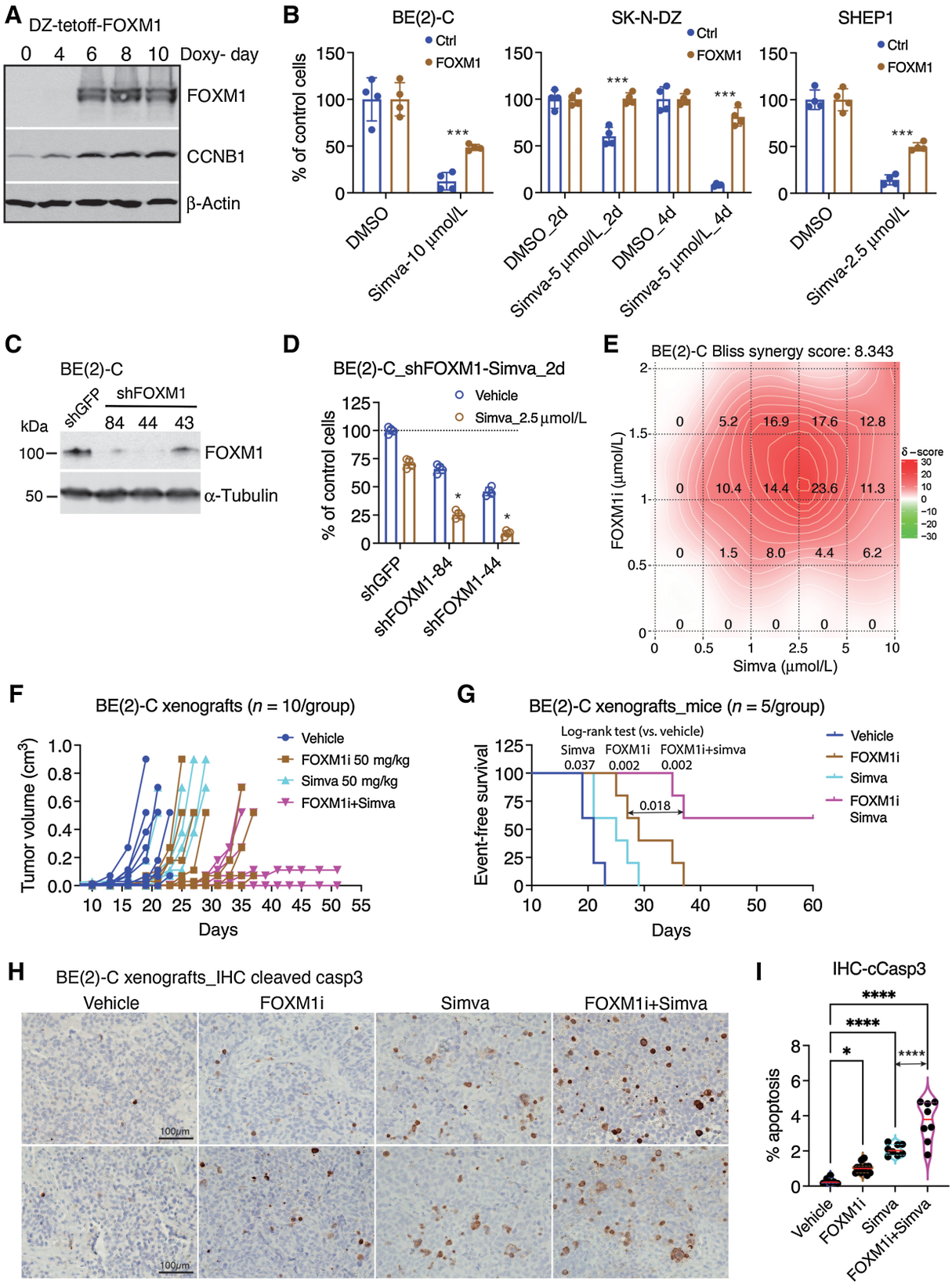
A
DZ-tetoff-FOXM1
0 4 6 8 10 Doxy- day
FOXM1
CCNB1
β-Actin
B
BE(2)-C
SK-N-DZ
SHEP1
Ctrl
FOXM1
% of control cells
DMSO
Simva-10 μmol/L
DMSO_2d
Simva-5 μmol/L_2d
DMSO_4d
Simva-5 μmol/L_4d
Simva-2.5 μmol/L
C
BE(2)-C
shGFP
shFOXM1
kDa
84 44 43
100
50
FOXM1
α-Tubulin
D
BE(2)-C_shFOXM1-Simva_2d
Vehicle
Simva_2.5 μmol/L
shGFP
shFOXM1-84
shFOXM1-44
E
BE(2)-C Bliss synergy score: 8.343
FOXM1i (μmol/L)
Simva (μmol/L)
δ–score
F
BE(2)-C xenografts (n = 10/group)
Tumor volume (cm3)
Days
Vehicle
FOXM1i 50 mg/kg
Simva 50 mg/kg
FOXM1i+Simva
G
BE(2)-C xenografts_mice (n = 5/group)
Log-rank test (vs. vehicle)
Simva FOXM1i FOXM1i+simva
0.037 0.002 0.002
0.018
Event-free survival
Days
Vehicle
FOXM1i
Simva
FOXM1i Simva
H
BE(2)-C xenografts_IHC cleaved casp3
Vehicle
FOXM1i
Simva
FOXM1i+Simva
100μm
I
IHC-cCasp3
% apoptosis
Vehicle
FOXM1i
Simva
FOXM1i+Simva

(**Fig. 3D**) and *MYCN*-amplified neuroblastoma cell lines (**Fig. 3E**). Comprehensive analysis using the Bliss model showed an average synergy score of 13.66 for BE(2)-C cells and 11.55 for IMR5 cells (**Fig. 3F**), indicating that the drug combination exhibited an overall synergistic anti-growth effect in the tested dose ranges. We obtained essentially the same results using a different synergy reference method, the high single agent (HSA) model (**Fig. 3G**). In non–*MYCN*-amplified SK-N-AS and SHEP1 cell lines, the drug combination generated an average Bliss synergy score of 6.58 for SK-N-AS cells and 8.08 for SHEP1 cells (Supplementary Fig. S6A), indicative of additive effects. However, synergistic interactions could be obtained at select doses (Supplementary Fig. S6A and S6B). The highest Bliss synergy score was 12.6 for SK-N-AS cells and 16.0 for SHEP1 cells (Supplementary Fig. S6A).

We further tested the drug combination in the PDX model of COG-N-519x, which was derived from a chemoresistant stage 4 neuroblastoma with *MYCN* amplification (19). NOD/SCID mice carrying COG-N-519x xenografts were randomly assigned to 5 groups and treated with vehicle, caffeinated drinking water (0.4 g caffeine/L, ∼80 mg/kg body weight daily), simvastatin at 50 mg/kg by gavage, or combination of simvastatin (50 mg/kg) with caffeinated water (0.2 or 0.4 g caffeine/L, ∼40 or 80 mg/kg, respectively). In agreement with *in vitro* data, caffeinated water by itself showed no significant effect, and simvastatin alone significantly reduced PDX growth and extended the survival of PDX-bearing mice (**Fig. 4A** and **B**). For combination treatment, caffeinated water at 40 mg/kg daily showed no effect but at 80 mg/kg significantly enhanced the efficacy of simvastatin (**Fig. 4A** and **B**). The treatment at the indicated doses and time had no significant effect on the mouse body weight (Supplementary Fig. S6C). IHC staining showed that simvastatin and its combination with caffeine markedly increased apoptosis in PDX tumors (**Fig. 4C** and **D**).

Collectively, these findings suggest that the combination of simvastatin and caffeine is a potentially effective therapy for *MYCN*-amplified neuroblastoma.

Caffeine synergizes with simvastatin via its activity as an adenosine receptor antagonist

Next, we wanted to identify the activity of caffeine specific to its synergistic interaction with simvastatin. Caffeine is structurally related to adenosine and functions primarily as an antagonist of adenosine receptors (43). There are also reports that caffeine functions as an antagonist of gamma-aminobutyric acid (GABA) receptors and a regulator of ER calcium levels (increasing ER calcium levels; ref. 27). Accordingly, we tested several compounds for their ability to abrogate the synergic effect of caffeine, including adenosine (adenosine receptor agonist), baclofen (GABA receptor agonist; ref. 44), and thapsigargin (reducing ER calcium levels by inhibiting sarco-ER Ca^{2+} ATPase that pumps Ca^{2+} ions from the cytosol into the ER; ref. 45). Immunoblot analysis revealed that only adenosine significantly abolished the effect of caffeine, restoring statin-induced feedback activation of mevalonate pathway enzymes (**Fig. 5A**). In addition, supplemental adenosine abrogated the ability of caffeine to enhance the anti-growth effect of simvastatin (**Fig. 5B**). These observations suggest that antagonizing adenosine receptors is a major mechanism for caffeine to synergize with simvastatin.

The A_{2A} adenosine receptor has the highest affinity to adenosine (43). Therefore, we asked whether the A_{2A} receptor antagonist KW-6002, also known as istradefylline (an add-on drug for Parkinson's disease), can phenocopy caffeine to enhance the anti-growth activity of simvastatin. Immunoblot analysis revealed that, like caffeine, KW-6002 diminished simvastatin-induced Srebp2 activation in CHO-K1 cells (**Fig. 5C**) and upregulation of ACSS2 and HMGCS1 in neuroblastoma IMR5 cells (**Fig. 5D**). Moreover, single-dose combination assays showed that KW-6002 synergized with simvastatin to inhibit the growth of neuroblastoma cell lines (**Fig. 5E**) and neuroblastoma PDX cells (Supplementary Fig. S7A). We further performed multiple-dose combination assays in three *MYCN*-amplified neuroblastoma cell lines and the data were analyzed using both Bliss and HSA reference models. All showed synergistic interactions between simvastatin and KW-6002 except the BE(2)-C-Bliss dataset (**Fig. 5F**; Supplementary Fig. S7B). The BE(2)-C-Bliss dataset showed an average score of 7.78, indicating an overall additive effect. However, synergy (Bliss score of 12.4) was observed when simvastatin in the range of 5 to 10 μmol/L was combined with KW-6002 in the range of 2.5 to 5.0 μmol/L (**Fig. 5F**, left). We obtained essentially the same results with the non–*MYCN*-amplified SK-N-AS cells. Both single- and multiple-dose assays demonstrated synergistic interactions between simvastatin and KW-6002, using either Bliss or HSA model analysis (Supplementary Fig. S7C–S7E).

SREBP2 activation requires its translocation from the ER to the Golgi (6). It has been shown recently that caffeine blocks SREBP2 activation by elevating ER Ca^{2+} levels to promote GRP78-mediated SREBP2 retention in the ER (27). We found that, like caffeine, KW-6002 treatment also elevated ER Ca^{2+} levels (**Fig. 5G** and **H**), as determined using the cell lines expressing D1ER, an ER Ca^{2+} sensor that displays increased fluorescence intensity when binding to Ca^{2+} (27, 28). This observation suggests a common mechanism for caffeine and KW-6002 to suppress the statin-induced feedback activation of SREBP2 by increasing ER Ca^{2+} levels.

Taken together, the data presented above provide evidence in support of the model that blocking adenosine receptor signaling is a major mechanism for the synergistic interaction of caffeine and simvastatin.

Discussion

High-risk neuroblastoma tumors display transcriptional activation of the mevalonate pathway, as evidenced by increased mRNA

Figure 2.

FOXM1 regulates the sensitivity of neuroblastoma cells to simvastatin. **A,** Immunoblot analysis of FOXM1 and its target cyclin B1 (CCNB1) in SK-N-DZ cells with inducible FOXM1 expression in the absence of doxycycline (Doxy-). β-actin levels are shown as loading control. **B,** Cell growth assays of neuroblastoma cell lines without or with FOXM1 induction that were treated with DMSO or simvastatin. FOXM1 induction conferred resistance to simvastatin. *P* values were determined by two-tailed Student *t* test. **C,** Immunoblot analysis of shRNA-mediated FOXM1 knockdown in BE(2)-C cells. α-Tubulin levels are shown as loading control. **D,** Cell growth assays of BE (2)-C cells without (shGFP) or with FOXM1 knockdown (shFOXM1) that were treated with DMSO or simvastatin. Synergistic effect determined by the Bliss reference model. **E,** Two-dimensional synergy plot showing additive or synergistic interaction between simvastatin and thiostrepton (FOXM1i), with indicated Bliss synergy scores: <10, additive effect; >10, synergistic effect. **F** and **G,** Tumor growth (**F**) and event-free survival (**G**) curves for NOD/SCID mice bearing BE (2)-C xenografts treated with vehicle, FOXM1i, simvastatin, or combination of simvastatin and FOXM1i. Treatment was started on the day of inoculation and ended on day 50 post-inoculation. Log-rank test *P* values are indicated for individual or combination of the drugs versus vehicle and drug combination versus FOXM1i. **H,** Representative images of IHC staining of cleaved caspase-3 from two xenografts treated with vehicle, FOXM1i, simvastatin, or combination of FOXM1i and simvastatin. **I,** Violin plot of apoptosis levels quantified as areas of cleaved caspase-3–positive staining in 8–10 IHC images (200×) from 2–3 xenografts per group. *P* values were determined by one-way ANOVA. *, $P < 0.05$; ***, $P < 0.001$; ****, $P < 0.0001$.

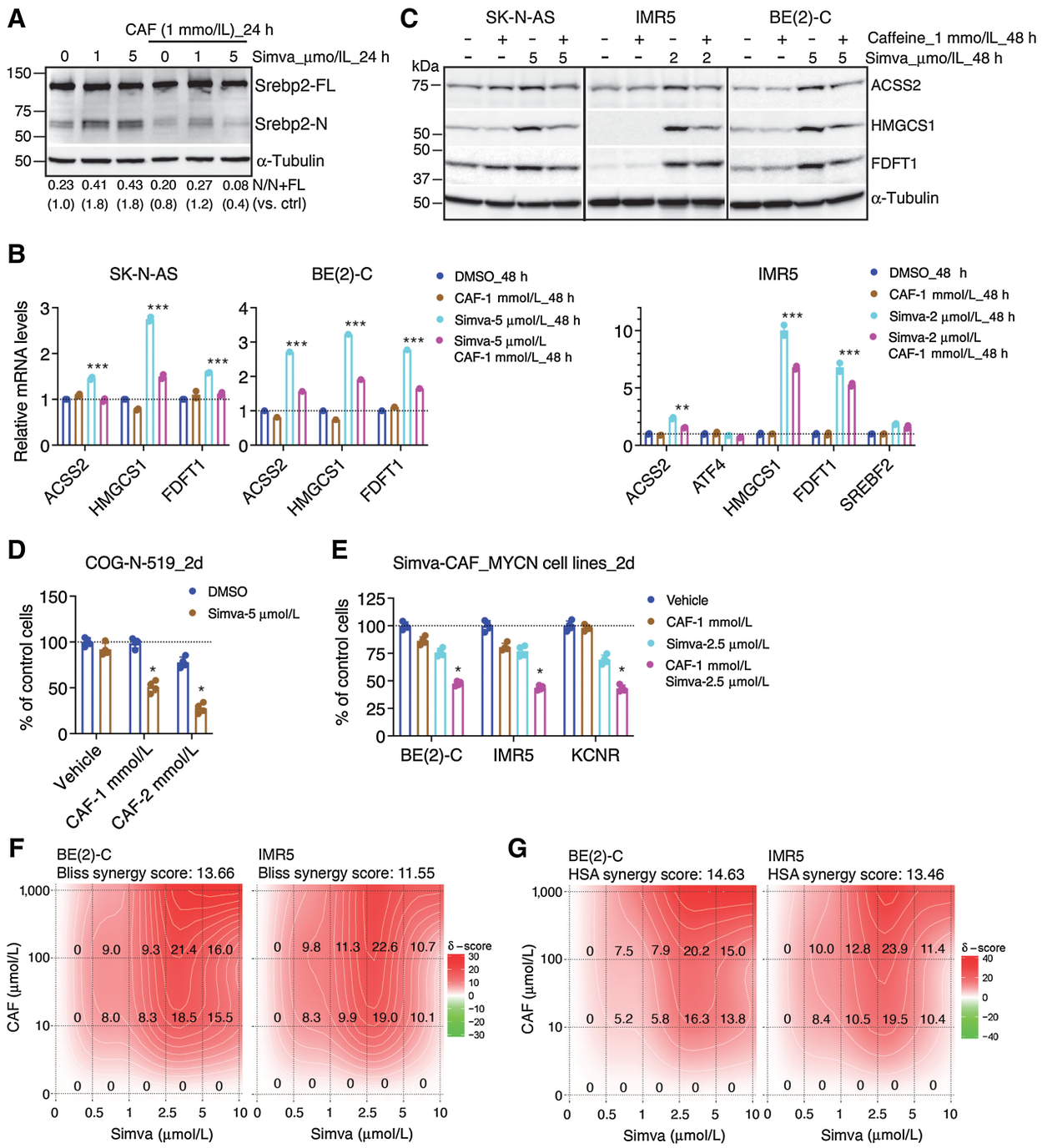

Figure 3.

Caffeine synergizes with simvastatin by blocking feedback activation of the mevalonate pathway. **A,** Immunoblot analysis of simvastatin-induced Srebp2 processing in CHO-K1 cells, which was blocked by caffeine (CAF). Srebp2-FL, full-length Srebp2 precursor; Srebp2-N, N-terminal Srebp2 with transcriptional activity. **B** and **C,** qRT-PCR (**B**) and immunoblot (**C**) analyses showing abrogation by caffeine of simvastatin-mediated upregulation of mevalonate pathway enzymes. Statistical significance was determined by two-tailed Student *t* test. **D** and **E,** Cell growth assays of PDX neuroblastoma cells (**D**) and *MYCN*-amplified neuroblastoma cell lines (**E**) treated with DMSO, caffeine, simvastatin, or combination of simvastatin and caffeine. Synergistic effect determined by the Bliss reference model. **F** and **G,** Two-dimensional synergy plots showing synergistic interaction between simvastatin and caffeine, with indicated Bliss (**F**) and HSA (**G**) synergy scores: > 10, synergistic. *, $P < 0.05$; **, $P < 0.01$; ***, $P < 0.001$.

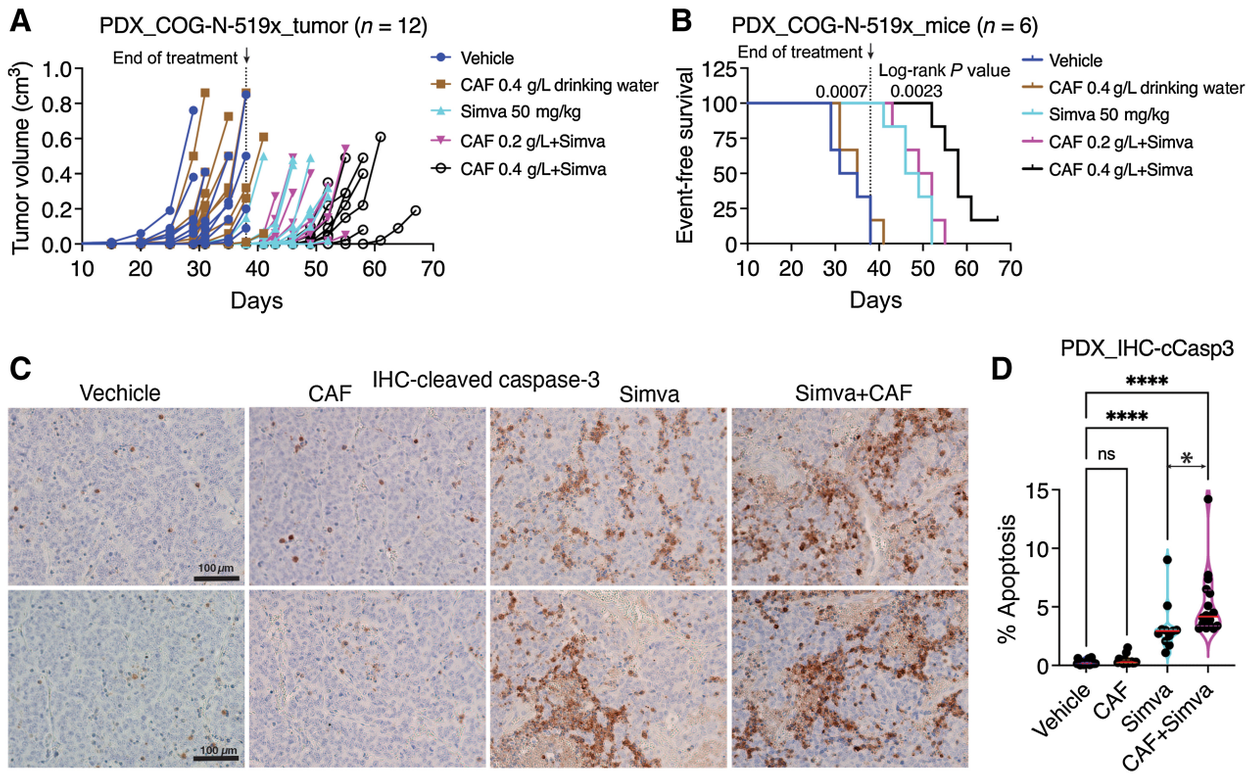

Figure 4.

Caffeine synergizes with simvastatin to inhibit PDX growth. **A** and **B,** Tumor growth (**A**) and event-free survival (**B**) curves for NOD/SCID mice bearing COG-N-519x PDX treated with vehicle, caffeinated water (0.4 g/L), simvastatin, or caffeinated water (0.2 g/L or 0.4 g/L) in combination with simvastatin. Treatment was started on the day of inoculation and ended on day 38 postinoculation. Log-rank test *P* values are indicated for simvastatin vs. vehicle and caffeinated water (0.4 g/L) plus simvastatin vs. simvastatin. **C,** Representative images of IHC staining of cleaved caspase-3 from two PDXs treated with vehicle, caffeinated water (0.4 g/L), simvastatin, or caffeinated water (0.4 g/L) in combination with simvastatin. **D,** Violin plot of apoptosis levels quantified as areas of cleaved caspase-3–positive staining in 8–10 IHC images (200×) from 2–3 xenografts per group. *P* values were determined by one-way ANOVA. ns, nonsignificant; *, $P < 0.05$: ****, $P < 0.0001$. CAF, caffeine.

expression of the genes that encode key enzymes of this pathway (10). In this report, we show that both the cholesterol and nonsterol GGPP branches of the mevalonate pathway are critical to sustain the survival and growth of neuroblastoma cells. Moreover, blocking the mevalonate pathway by simvastatin significantly decreases spontaneous neuroblastoma development in the *TH-MYCN* mouse model and impedes neuroblastoma PDX growth. These findings underscore the potential of the mevalonate pathway as a therapeutic target for high-risk neuroblastoma.

Mechanistically, we show that a key function of the mevalonate pathway is to maintain the expression of FOXM1 and its target genes responsible for driving M phase progression (39). Our data are consistent with a recent study in liver cancer cell lines showing that statin represses FOXM1 expression by blocking geranylgeranylation of RhoA, Rac1 or Cdc42 proteins (46). Together, these findings suggest a molecular mechanism for the long-observed connection between the mevalonate pathway and cell-cycle progression (47). It should be mentioned that there is also evidence suggesting that cholesterol is essential for M phase progression (47). It was found about 50 years ago that HMGCR inhibition blocks cell proliferation, which can be rescued by supplemental cholesterol (48, 49). More recently, it was reported that blocking cholesterol synthesis reduces CDK1 activity and arrests cells in the G_2–M phase, which again can be abolished by supplemental cholesterol (50). The molecular mechanism for linking cholesterol to FOXM1 and mitotic gene expression remains to be determined.

High FOXM1 expression is observed in many types of cancer (37) and is most frequently associated with adverse risk across 39 malignancies (51). We have reported similar findings with neuroblastoma (39). Our current study provides evidence for increased FOXM1 expression as a potential cause of statin resistance, as FOXM1 overexpression markedly reduces the sensitivity of neuroblastoma cells to statins. Moreover, we show that the connection between the mevalonate pathway and FOXM1 provides a therapeutic opportunity: Statin treatment sensitizes neuroblastoma cells to FOXM1 inhibition. Although the combination of simvastatin and thiostrepton shows an overall additive effect, synergy can be achieved within a specific range of concentrations. Also, it is important to recognize that even additive effects can be beneficial therapeutically (52, 53). In support of this notion, we found that a combination of simvastatin and thiostrepton (a FOXM1 inhibitor) displays a significantly more robust antitumor effect compared with either drug alone in a neuroblastoma xenograft model. It is well established that targeting the same gene or protein via multiple ways is a rational approach to enhance activity or to overcome resistance (53, 54). Thus, we speculate that other drugs that target mitosis may also show additive or synergistic effects in combination with statins.

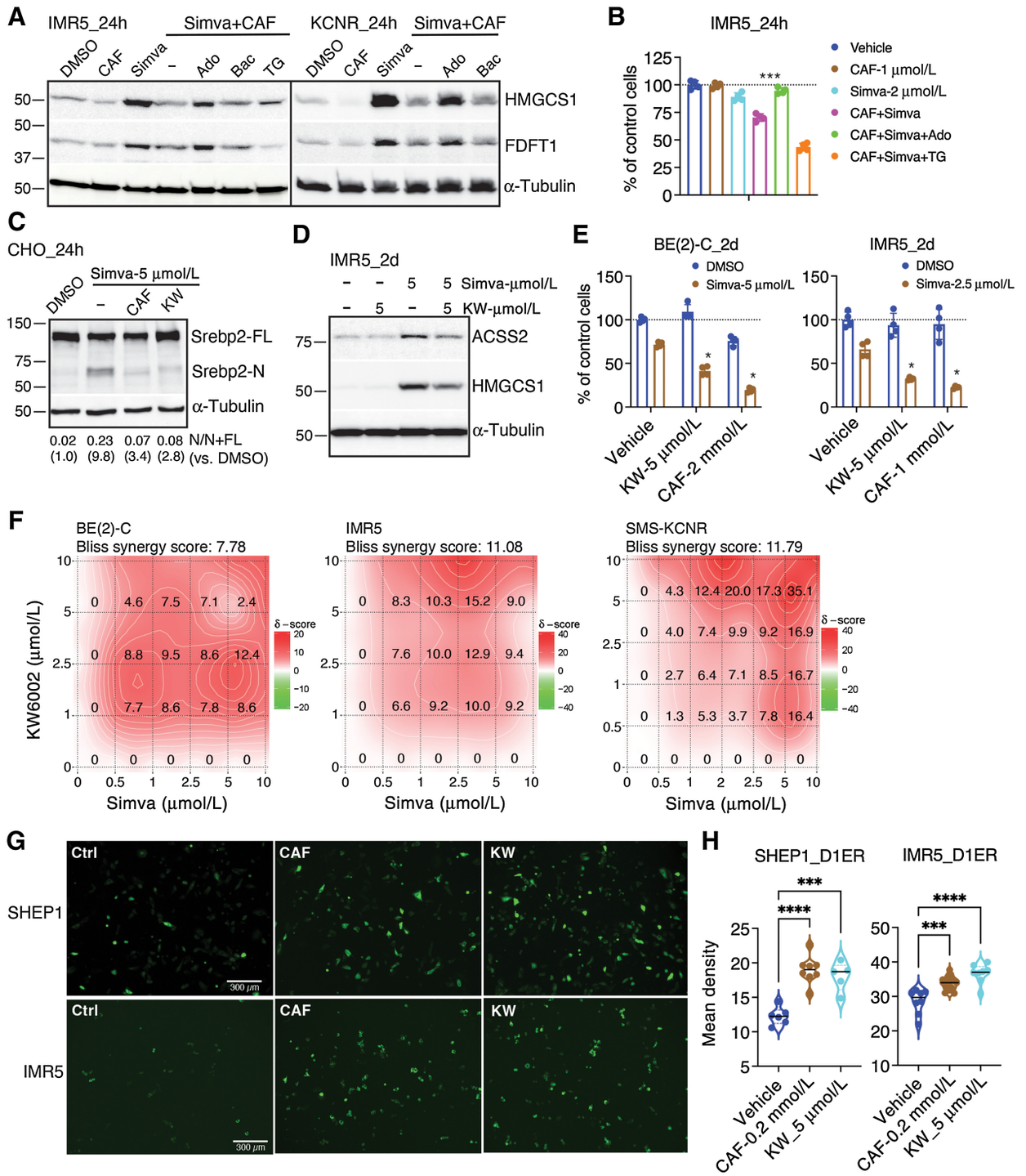

Figure 5.

Caffeine acts as an adenosine receptor antagonist to augment the effect of simvastatin. **A** and **B,** Supplemental adenosine (Ado), but not other compounds, abolishes the ability of caffeine to block simvastatin-induced mevalonate pathway enzymes (**A**) and to sensitize cells to simvastatin (**B**). Bac, Baclofen; TG, thapsigargin. *P* values were determined by two-tailed Student *t* test. **C** and **D,** Immunoblot analysis shows abrogation of simvastatin-induced Srebp2 processing in CHO-K1 cells (**C**) and upregulation of mevalonate pathway enzymes in IMR5 cells (**D**) by the adenosine receptor antagonist KW6002. **E,** Cell growth assays of neuroblastoma cell lines treated for 48 hours with DMSO, KW6002, caffeine, simvastatin, or simvastatin plus KW6002 or caffeine. Synergistic effect determined by the Bliss reference model. **F,** Two-dimensional synergy plots showing synergistic interaction between simvastatin and KW6002 in *MYCN*-amplified neuroblastoma cell lines, with indicated Bliss synergy scores: > 10, synergistic. **G,** Representative fluorescence images of neuroblastoma cells expressing the FRET-based ER Ca^{2+} sensor D1ER following treatment with vehicle (Ctrl), 0.2 mmol/L caffeine, or 5 µmol/L KW6002 for 24 hours. **H,** Violin plots of fluorescent intensity quantified from 5 to 15 fluorescent microscope images (200×) of at least three biological replicates. *P* values were determined by one-way ANOVA. *, $P < 0.05$; ***, $P < 0.001$; ****, $P < 0.0001$. CAF, caffeine.

Upregulation of drug target expression is a major mode of resistance (54). Similar to the sterol depletion-induced feedback response (55), statin treatment triggers activation of SREBP2 and transcriptional upregulation of mevalonate pathway enzymes, which has been shown to be a mechanism for statin resistance (40, 41). Combining drugs to disrupt this feedback loop is a strategy to overcome the resistance (4). Studies from the Penn laboratory have shown that dipyridamole, an FDA-approved drug for preventing blood clots and stroke (56), can synergistically enhance the antitumor effect of statins by blocking statin-mediated feedback activation of SREBP2 and the mevalonate pathway (41, 57). More recently, it was reported that dipyridamole prevents the ER to Golgi translocation of the SCAP-SREBP2 complex (58), which is required for the processing and activation of SREBP2 (6).

Our investigation uncovers a new class of agents to boost the antitumor effect of statins. We show that caffeine, the most widely consumed psychoactive agent found in coffee and tea (59), can synergize with simvastatin to suppress the growth of *MYCN*-amplified neuroblastoma cell lines and PDX cells in culture. Moreover, we show that caffeine at the dose of ∼80 mg/kg body weight daily enhances the antitumor effect of simvastatin in a neuroblastoma PDX mouse model. Using the FDA algorithm for calculating human equivalent dose (HED) based on the body surface area (60), we estimated that the mouse dose of 80 mg/kg is the HED of 6.5 mg/kg. According to the 2001 Institute of Medicine study (61), mean daily intake for the top 10% of adult caffeine users is about 5–7 mg/kg, suggesting that the effective caffeine dose in our study is safe for humans.

Like dipyridamole (41, 57), caffeine can block statin-induced feedback activation of SREBP2 and mevalonate pathway enzymes. Our data suggest that this action of caffeine depends on its activity as an antagonist of adenosine receptors (43, 59, 62), as evidenced by the findings that supplemental adenosine can abrogate the ability of caffeine to block statin-induced feedback activation SREBP2 and mevalonate pathway enzymes and to enhance the antigrowth effect of simvastatin. In further support of this model, we found that the A_{2A} adenosine receptor antagonist KW-6002 (istradefylline, brand name Nourianz) can phenocopy the action of caffeine and synergize with simvastatin to repress neuroblastoma cell growth. These findings provide a strong rationale for evaluating other adenosine receptor antagonists for their capacity to enhance the antitumor effect of statins.

In summary, we present evidence that simvastatin can inhibit neuroblastoma growth in *TH-MYCN* and PDX mouse models. Furthermore, we identify two classes of agents, caffeine (and adenosine receptor antagonists) and FOXM1 inhibitors, to boost the antitumor effect of statins and to overcome statin resistance. Our findings provide a rationale for their combinations as a cancer therapeutic strategy.

Limitations of the study

Our statin treatment began on the day of tumor cell inoculation for xenograft models or on postnatal day 31 for *TH-MYCN* mice when neuroblastoma development was most likely in the precancerous stage characterized by multifocal hyperplasia (16, 32). Whether statins are effective against advanced tumors remains to be investigated. In addition, our drug combination assays were conducted with simvastatin in limited concentration ranges. Further studies are needed to test other statins and to define optimal drug combinations for maximal therapeutic efficacy.

Authors' Disclosures

J. Ding reports grants from NIH during the conduct of the study. S. Sudarshan reports grants from NIH outside the submitted work. H.F. Ding reports grants from NIH during the conduct of the study. No disclosures were reported by the other authors.

Authors' Contributions

G.B. Tran: Conceptualization, software, formal analysis, investigation, methodology, writing–original draft. **J. Ding:** Conceptualization, formal analysis, supervision, validation, investigation, methodology, writing–original draft, project administration. **B. Ye:** Formal analysis, investigation. **M. Liu:** Formal analysis, investigation. **Y. Yu:** Formal analysis, investigation. **Y. Zha:** Resources, supervision, investigation. **Z. Dong:** Resources, formal analysis, experimental design and providing reagents. **K. Liu:** Resources, formal analysis, experimental design and providing reagents. **S. Sudarshan:** Resources, formal analysis, experimental design and data interpretation. **H.F. Ding:** Conceptualization, data curation, formal analysis, supervision, funding acquisition, validation, investigation, writing–original draft, writing–review and editing.

Acknowledgments

The authors thank John Ness and Dr. Dezhi Wang in the Pathology Core Research Lab at the University of Alabama at Birmingham (UAB) for IHC studies, Drs. Mythreye Karthikeyan, John C. Kappes, and Haitao Ding (UAB) for providing CHO cell lines, C Patrick Reynolds (Children's Oncology Group, Texas Tech University) for providing neuroblastoma PDXs, Justin Choi (National Marine Biodiversity Institute of Korea) for GSEA, and Rogier Versteeg and the Department of Oncogenomics at the Academic Medical Center (Amsterdam, The Netherlands) for the R2 Genomics Analysis and Visualization Platform. S. Sudarshan is supported by NIH R01CA200653 and Department of Veterans Affairs I01BX002930. Z. Dong is a VA senior research career scientist. The work was supported by a grant from NIH (R01CA236890) to H.F. Ding.

The publication costs of this article were defrayed in part by the payment of publication fees. Therefore, and solely to indicate this fact, this article is hereby marked "advertisement" in accordance with 18 USC section 1734.

Note

Supplementary data for this article are available at Cancer Research Online (http://cancerres.aacrjournals.org/).

Received November 2, 2022; revised March 14, 2023; accepted April 12, 2023; published first April 14, 2023.

References

1. Goldstein JL, Brown MS. Regulation of the mevalonate pathway. Nature 1990; 343:425–30.
2. Mullen PJ, Yu R, Longo J, Archer MC, Penn LZ. The interplay between cell signaling and the mevalonate pathway in cancer. Nat Rev Cancer 2016; 16:718–31.
3. van Meer G, Voelker DR, Feigenson GW. Membrane lipids: where they are and how they behave. Nat Rev Mol Cell Biol 2008;9:112–24.
4. Longo J, van Leeuwen JE, Elbaz M, Branchard E, Penn LZ. Statins as anticancer agents in the era of precision medicine. Clin Cancer Res 2020;26:5791–800.
5. Juarez D, Fruman DA. Targeting the mevalonate pathway in cancer. Trends Cancer 2021;7:525–40.
6. Goldstein JL, DeBose-Boyd RA, Brown MS. Protein sensors for membrane sterols. Cell 2006;124:35–46.
7. Cohn SL, Pearson ADJ, London WB, Monclair T, Ambros PF, Brodeur GM, et al. The international neuroblastoma risk group (INRG) classification system: an INRG task force report. J Clin Oncol 2009;27:289–97.
8. Qiu B, Matthay KK. Advancing therapy for neuroblastoma. Nat Rev Clin Oncol 2022;19:515–33.

9. Bansal M, Gupta A, Ding H-F. MYCN and metabolic reprogramming in neuroblastoma. Cancers 2022;14:4113.
10. Liu M, Xia Y, Ding J, Ye B, Zhao E, Choi JH, et al. Transcriptional profiling reveals a common metabolic program in high-risk human neuroblastoma and mouse neuroblastoma sphere-forming cells. Cell Rep 2016;17:609–23.
11. Stokes ME, Small JC, Vasciaveo A, Shimada K, Hirschhorn T, Califano A, et al. Mesenchymal subtype neuroblastomas are addicted to TGF-βR2/HMGCR-driven protein geranylgeranylation. Sci Rep 2020;10:10748.
12. Kuzyk CL, Anderson CC, Roede JR. Simvastatin induces delayed apoptosis through disruption of glycolysis and mitochondrial impairment in neuroblastoma cells. Clin Transl Sci 2020;13:563–72.
13. Alizadeh J, Zeki AA, Mirzaei N, Tewary S, Rezaei Moghadam A, Glogowska A, et al. Mevalonate cascade inhibition by simvastatin induces the intrinsic apoptosis pathway via depletion of isoprenoids in tumor cells. Sci Rep 2017;7:44841.
14. Dimitroulakos J, Yeger H. HMG-CoA reductase mediates the biological effects of retinoic acid on human neuroblastoma cells: lovastatin specifically targets P-glycoprotein-expressing cells. Nat Med 1996;2:326–33.
15. Xia Y, Ye B, Ding J, Yu Y, Alptekin A, Thangaraju M, et al. Metabolic reprogramming by MYCN confers dependence on the serine-glycine-one-carbon biosynthetic pathway. Cancer Res 2019;79:3837–50.
16. Alam G, Cui H, Shi H, Yang L, Ding J, Mao L, et al. MYCN promotes the expansion of Phox2B-positive neuronal progenitors to drive neuroblastoma development. Am J Pathol 2009;175:856–66.
17. Stewart E, Federico SM, Chen X, Shelat AA, Bradley C, Gordon B, et al. Orthotopic patient-derived xenografts of pediatric solid tumors. Nature 2017;549:96–100.
18. Siraj AK, Pratheeshkumar P, Parvathareddy SK, Qadri Z, Thangavel S, Ahmed S, et al. FoxM1 is an independent poor prognostic marker and therapeutic target for advanced Middle Eastern breast cancer. Oncotarget 2018;9:17466–82.
19. Harenza JL, Diamond MA, Adams RN, Song MM, Davidson HL, Hart LS, et al. Transcriptomic profiling of 39 commonly used neuroblastoma cell lines. Scientific Data 2017;4:170033.
20. Zhang W, Yu Y, Hertwig F, Thierry-Mieg J, Zhang W, Thierry-Mieg D, et al. Comparison of RNA-seq and microarray-based models for clinical endpoint prediction. Genome Biol 2015;16:133.
21. Rajbhandari P, Lopez G, Capdevila C, Salvatori B, Yu J, Rodriguez-Barrueco R, et al. Cross-cohort analysis identifies a TEAD4-MYCN positive feedback loop as the core regulatory element of high-risk neuroblastoma. Cancer Discov 2018;8:582–99.
22. Mao L, Ding J, Zha Y, Yang L, McCarthy BA, King W, et al. HOXC9 links cell-cycle exit and neuronal differentiation and is a prognostic marker in neuroblastoma. Cancer Res 2011;71:4314–24.
23. Wang X, Yang L, Choi JH, Kitamura E, Chang CS, Ding J, et al. Genome-wide analysis of HOXC9-induced neuronal differentiation of neuroblastoma cells. Genom Data 2014;2:50–2.
24. Ianevski A, Giri AK, Aittokallio T. SynergyFinder 2.0: visual analytics of multi-drug combination synergies. Nucleic Acids Res 2020;48:W488–W93.
25. Ianevski A, Giri AK, Gautam P, Kononov A, Potdar S, Saarela J, et al. Prediction of drug combination effects with a minimal set of experiments. Nat Mach Intell 2019;1:568–77.
26. Borisy AA, Elliott PJ, Hurst NW, Lee MS, Lehár J, Price ER, et al. Systematic discovery of multicomponent therapeutics. Proc Natl Acad Sci USA 2003;100:7977–82.
27. Lebeau PF, Byun JH, Platko K, Saliba P, Sguazzin M, MacDonald ME, et al. Caffeine blocks SREBP2-induced hepatic PCSK9 expression to enhance LDLR-mediated cholesterol clearance. Nat Commun 2022;13:770.
28. Palmer AE, Jin C, Reed JC, Tsien RY. Bcl-2-mediated alterations in endoplasmic reticulum Ca2+ analyzed with an improved genetically encoded fluorescent sensor. Proc Natl Acad Sci USA 2004;101:17404–9.
29. Weiss WA, Aldape K, Mohapatra G, Feuerstein BG, Bishop JM. Targeted expression of MYCN causes neuroblastoma in transgenic mice. Embo J 1997;16:2985–95.
30. Moore HC, Wood KM, Jackson MS, Lastowska MA, Hall D, Imrie H, et al. Histological profile of tumors from MYCN transgenic mice. J Clin Pathol 2008;61:1098–103.
31. Teitz T, Stanke JJ, Federico S, Bradley CL, Brennan R, Zhang J, et al. Preclinical models for neuroblastoma: establishing a baseline for treatment. PLoS One 2011;6:e19133.
32. Hansford LM, Thomas WD, Keating JM, Burkhart CA, Peaston AE, Norris MD, et al. Mechanisms of embryonal tumor initiation: distinct roles for MycN expression and MYCN amplification. Proc Natl Acad Sci USA 2004;101:12664–9.
33. Chabner BA, Roberts TG. Chemotherapy and the war on cancer. Nat Rev Cancer 2005;5:65–72.
34. Wang M, Casey PJ. Protein prenylation: unique fats make their mark on biology. Nat Rev Mol Cell Biol 2016;17:110–22.
35. Kwok JM, Myatt SS, Marson CM, Coombes RC, Constantinidou D, Lam EW. Thiostrepton selectively targets breast cancer cells through inhibition of forkhead box M1 expression. Mol Cancer Ther 2008;7:2022–32.
36. Hegde NS, Sanders DA, Rodriguez R, Balasubramanian S. The transcription factor FOXM1 is a cellular target of the natural product thiostrepton. Nat Chem 2011;3:725–31.
37. Sadasivam S, DeCaprio JA. The DREAM complex: master coordinator of cell cycle–dependent gene expression. Nat Rev Cancer 2013;13:585–95.
38. Wang Z, Park HJ, Carr JR, Chen YJ, Zheng Y, Li J, et al. FoxM1 in tumorigenicity of the neuroblastoma cells and renewal of the neural progenitors. Cancer Res 2011;71:4292–302.
39. Zha Y, Xia Y, Ding J, Choi JH, Yang L, Dong Z, et al. MEIS2 is essential for neuroblastoma cell survival and proliferation by transcriptional control of M-phase progression. Cell Death Dis 2014;5:e1417.
40. Göbel A, Breining D, Rauner M, Hofbauer LC, Rachner TD. Induction of 3-hydroxy-3-methylglutaryl-CoA reductase mediates statin resistance in breast cancer cells. Cell Death Dis 2019;10:91.
41. Longo J, Mullen PJ, Yu R, van Leeuwen JE, Masoomian M, Woon DTS, et al. An actionable sterol-regulated feedback loop modulates statin sensitivity in prostate cancer. Mol Metab 2019;25:119–30.
42. Adams CM, Reitz J, De Brabander JK, Feramisco JD, Li L, Brown MS, et al. Cholesterol and 25-hydroxycholesterol inhibit activation of SREBPs by different mechanisms, both involving SCAP and insigs. J Biol Chem 2004;279:52772–80.
43. Chen JF, Eltzschig HK, Fredholm BB. Adenosine receptors as drug targets–what are the challenges? Nat Rev Drug Discov 2013;12:265–86.
44. Hudgson P, Weightman D. Baclofen in the treatment of spasticity. Br Med J 1971;4:15–7.
45. Doan NTQ, Paulsen ES, Sehgal P, Møller JV, Nissen P, Denmeade SR, et al. Targeting thapsigargin towards tumors. Steroids 2015;97:2–7.
46. Ogura S, Yoshida Y, Kurahashi T, Egawa M, Furuta K, Kiso S, et al. Targeting the mevalonate pathway is a novel therapeutic approach to inhibit oncogenic FoxM1 transcription factor in human hepatocellular carcinoma. Oncotarget 2018;9:21022–35.
47. Lasunción MA, Martínez-Botas J, Martín-Sánchez C, Busto R, Gómez-Coronado D. Cell cycle dependence on the mevalonate pathway: role of cholesterol and nonsterol isoprenoids. Biochem Pharmacol 2022;196:114623.
48. Brown MS, Goldstein JL. Suppression of 3-Hydroxy-3-methylglutaryl coenzyme a reductase activity and inhibition of growth of human fibroblasts by 7-keto-cholesterol. J Biol Chem 1974;249:7306–14.
49. Chen HW, Kandutsch AA, Waymouth C. Inhibition of cell growth by oxygenated derivatives of cholesterol. Nature 1974;251:419–21.
50. Martínez-Botas J, Suárez Y, Ferruelo AJ, Gómez-Coronado D, Lasuncion MA. Cholesterol starvation decreases p34(cdc2) kinase activity and arrests the cell cycle at G2. Faseb j 1999;13:1359–70.
51. Gentles AJ, Newman AM, Liu CL, Bratman SV, Feng W, Kim D, et al. The prognostic landscape of genes and infiltrating immune cells across human cancers. Nat Med 2015;21:938–45.
52. Lopez JS, Banerji U. Combine and conquer: challenges for targeted therapy combinations in early phase trials. Nat Rev Clin Oncol 2017;14:57–66.
53. Jia J, Zhu F, Ma X, Cao ZW, Li YX, Chen YZ. Mechanisms of drug combinations: interaction and network perspectives. Nat Rev Drug Discov 2009;8:111–28.
54. Al-Lazikani B, Banerji U, Workman P. Combinatorial drug therapy for cancer in the post-genomic era. Nat Biotechnol 2012;30:679–92.
55. Brown MS, Goldstein JL. The SREBP pathway: regulation of cholesterol metabolism by proteolysis of a membrane-bound transcription factor. Cell 1997;89:331–40.
56. Schaper W. Dipyridamole, an underestimated vascular protective drug. Cardiovasc Drugs Ther 2005;19:357–63.

57. Pandyra A, Mullen PJ, Kalkat M, Yu R, Pong JT, Li Z, et al. Immediate utility of two approved agents to target both the metabolic mevalonate pathway and its restorative feedback loop. Cancer Res 2014;74:4772–82.
58. Esquejo RM, Roqueta-Rivera M, Shao W, Phelan PE, Seneviratne U, Am Ende CW, et al. Dipyridamole inhibits lipogenic gene expression by retaining SCAP-SREBP in the endoplasmic reticulum. Cell Chem Biol 2021;28:169–79.
59. van Dam RM, Hu FB, Willett WC. Coffee, caffeine, and health. N Engl J Med 2020;383:369–78.
60. U.S. Food and Drug Administration Center for Drug Evaluation and Research. Guidance for industry estimating the maximum safe starting dose in initial clinical trials for therapeutics in adult healthy volunteers. Rockville (MD): U.S. Food and Drug Administration; July 2005. p. 27. Available from: https://www.fda.gov/media/72309/download.
61. Medicine Io. Caffeine for the sustainment of mental task performance: formulations for military operations. Washington (DC): National Academies Press; 2001.
62. Sawynok J, Yaksh TL. Caffeine as an analgesic adjuvant: a review of pharmacology and mechanisms of action. Pharmacol Rev 1993;45:43–85.